This article was downloaded by: [McGill University Library]
On: 06 October 2012, At: 05:35
Publisher: Taylor & Francis
Informa Ltd Registered in England and Wales Registered Number: 1072954
Registered office: Mortimer House, 37-41 Mortimer Street, London W1T 3JH, UK


Numerical Heat Transfer, Part B: Fundamentals: An International Journal of Computation and Methodology
Publication details, including instructions for authors and subscription information:
http://www.tandfonline.com/loi/unhb20

# AUTOMATIC RESOLUTION CONTROL FOR THE FINITE-VOLUME METHOD, PART 1: A-POSTERIORI ERROR ESTIMATES

H. Jasak, A. D. Gosman

[a] Computational Dynamics Ltd., Hythe House, 200 Shepherds Bush Road, London W6 7NY, England

[b] Department of Mechanical Engineering, Imperial College of Science, Technology and Medicine, Exhibition Road, London SW7 2BX, England

Version of record first published: 29 Oct 2010.

To cite this article: H. Jasak, A. D. Gosman (2000): AUTOMATIC RESOLUTION CONTROL FOR THE FINITE-VOLUME METHOD, PART 1: A-POSTERIORI ERROR ESTIMATES, Numerical Heat Transfer, Part B: Fundamentals: An International Journal of Computation and Methodology, 38:3, 237-256

To link to this article: http://dx.doi.org/10.1080/10407790050192753

PLEASE SCROLL DOWN FOR ARTICLE

Full terms and conditions of use: http://www.tandfonline.com/page/terms-and-conditions

This article may be used for research, teaching, and private study purposes. Any substantial or systematic reproduction, redistribution, reselling, loan, sub-licensing, systematic supply, or distribution in any form to anyone is expressly forbidden.

The publisher does not give any warranty express or implied or make any representation that the contents will be complete or accurate or up to date. The accuracy of any instructions, formulae, and drug doses should be independently verified with primary sources. The publisher shall not be liable for any loss, actions, claims, proceedings, demand, or costs or damages whatsoever or howsoever caused arising directly or indirectly in connection with or arising out of the use of this material.

Downloaded by [McGill University Library] at 05:35 06 October 2012

Numerical Heat Transfer, Part B, 38:237–256, 2000
Copyright © 2000 Taylor & Francis
1040-7782/00 $12.00 + .00

Downloaded by [McGill University Library] at 05:35 06 October 2012

# AUTOMATIC RESOLUTION CONTROL FOR THE FINITE-VOLUME METHOD, PART 1: A-POSTERIORI ERROR ESTIMATES

***H. Jasak***
*Computational Dynamics Ltd., Hythe House, 200 Shepherds Bush Road, London W6 7NY, England*

***A. D. Gosman***
*Department of Mechanical Engineering, Imperial College of Science, Technology and Medicine, Exhibition Road, London SW7 2BX, England*

***Automatic Resolution Control, consisting of an a-posteriori error estimate and a local adjustment of the discretisation scheme, aims at producing a numerical solution of prescribed accuracy with minimum computational effort. In this paper, two a-posteriori error estimates concentrating on the absolute error levels are presented. The Taylor Series Error Estimate is based on a single-grid Taylor series truncation error analysis. The Moment Error Estimate is derived from the balance condition for the higher moments of the transported variable. Two error estimates are validated on two test cases with analytical solutions, where they typically bound the exact error.***

## 1. INTRODUCTION

Numerical solutions of fluid flow and heat transfer problems generally include three groups of errors [1]:

*Modeling errors*, defined as the difference between the actual flow and the exact solution of the mathematical model describing the behavior of the system in terms of coupled partial differential equations. For laminar flows, the mathematical model (Navier-Stokes equations) can be considered exact for engineering purposes; in turbulent, two-phase or reacting flows, the additional models do not always describe the underlying physical processes accurately and thus introduce potentially high modeling errors.

The second group of errors originates from the method used to solve the mathematical model. *Discretization errors* describe the difference between the exact solution of the system of algebraic equations obtained by discretizing the governing equations and the (usually unknown) exact solution of the mathematical model. Discretization errors depend on the accuracy of the equation discretization, as well as the discretization of the solution domain.

Received 11 January 2000; accepted 26 March 2000.
Address correspondence to Dr. Hrvoje Jasak, Computational Dynamics Ltd., Hythe House, 200 Shepherds Bush Road, London W6 7NY, England. E-mail: h.jasak@cd.co.uk

## NOMENCLATURE

| | | | |
|---|---|---|---|
| $a_N$ | matrix coefficient corresponding to the neighbor $N$ | $O(\mathbf{x})$ | higher-order truncation error |
| | | $P$ | center of the control volume |
| $a_P$ | central coefficient | $r_P$ | cell moment imbalance |
| $C(\mathbf{x})$ | leading term of the truncation error | $R_P$ | right-hand side of the algebraic equation |
| $\mathbf{d}$ | $\overline{PN}$ vector | $\mathbf{s}$ | face area vector |
| $D$ | diameter of the jet | $S_\phi$ | source term |
| $e$ | solution error | $S^*$ | point source intensity |
| $e_m$ | moment error estimate | $S$ | constant part of the source term |
| $e_t$ | Taylor series error estimate | $T$ | time scale |
| $f$ | face, face interpolate | $\mathbf{u}$ | velocity |
| $f_x$ | interpolation factor | $u_t$ | effective transport velocity |
| $F$ | face convection flux | $V$ | volume |
| $h$ | mesh size | $\mathbf{x}$ | position vector |
| $\mathbf{k}$ | nonorthogonal part of the face area vector | $\mathbf{1}, \mathbf{2}, \mathbf{3}$ | principal vectors of inertia |
| | | $\gamma$ | diffusivity |
| $K_0$ | Bessel function | $\Delta$ | orthogonal part of the face area vector |
| $L$ | linear part of the source term | | |
| $m_\phi$ | second moment of $\phi$ | $\phi$ | general tensorial property |
| $\mathbf{M}$ | second geometric moment tensor | $\Phi$ | exact solution |
| $N$ | center of the neighboring control volume | | |

Downloaded by [McGill University Library] at 05:35 06 October 2012

The system of algebraic equations constructed by discretization is usually solved with an iterative solver. The difference between the approximate and the exact solutions of the system is described by *convergence errors*. Errors caused by equation linearization or incomplete convergence over the set of coupled equations are also included here. Convergence errors can typically be reduced to an arbitrary level.

Early efforts in error detection for the finite-volume method (FVM) have been directed toward the problems with discontinuous solutions, such as multiple shock structures in supersonic flows [2–4]. Here, the solution has some distinct features that can be recognised by large gradients in flow variables. Combinations of gradients of flow variables are called *error indicators* and do not provide information about the absolute error level. A relatively wide selection of error indicators and the associated refinement procedures has been reported to date [5–12]. In problems with smooth solutions, the error cannot be controlled by an error indicator, as the presence of high gradients can be successfully rectified with mesh refinement. Additionally, refinement needs to be stopped when the desired accuracy is reached. Examples of *error estimates* that concentrate on the actual discretization error rather than the regions of high gradients can be found in, e.g., [13–24].

The ultimate purpose of an a-posteriori error estimate is to control an error-driven adaptive refinement algorithm in order to produce automatically a solution of prespecified numerical accuracy. A good error estimate therefore has the following properties: (1) the error is given in terms of the absolute error value;

(2) it provides reliable information about the distribution of the error; (3) it works well on coarse meshes; (4) scales correctly with the order of discretization and mesh size; (5) it is based on the local solution and mesh information and is cheap to compute; (6) it is applicable to all degenerate forms of the transport equation (elliptic, convection- or source-dominated problems); (7) it is asymptotically exact, i.e., it tends to the ''exact'' error faster than the solution tends to the exact solution; (8) it detects both the errors resulting from insufficient mesh resolution and the discretization errors from other sources (e.g., mesh quality, numerical diffusion); and (9) it modestly overestimates the actual error. Some of these properties are very difficult to achieve and some are even contradictive; the two error estimates presented here are a compromise between the requirements suggested above.

In this article we shall examine the problem of a-posteriori error estimation for the FVM. In order to understand the basics of the proposed error estimates, a short outline of the second-order-accurate FV discretization on arbitrarily unstructured meshes will be given [25]. Using this as a basis, two novel a-posteriori error estimates will be derived, namely, the Taylor series error estimate (TSEE), based on the Taylor series truncation error analysis (Section 3.2), and the moment error estimate (MEE), based on the higher moment balance (Section 4). The error estimates will be validated on two test cases with analytical solutions in Section 5, allowing us to compare the estimated and exact error levels.

In order to somewhat simplify the derivation of the error estimates and provide a complete picture of their accuracy, the rest of this article will concentrate only on the spatial component of the error. The extension of both error estimates to transient flows is relatively straightforward, but, as this should be accompanied by several illustrative examples, will be described separately.

Downloaded by [McGill University Library] at 05:35 06 October 2012

## 2. FINITE-VOLUME DISCRETIZATION

The discretization error depends on the applied discretization method, and it is therefore necessary to examine the basis of the descretization to be able to estimate the error correctly. A short outline of the FV discretization on arbitrarily unstructured meshes [25] is therefore given before we examine the options on error estimation.

Consider the standard form of a steady-state transport equation for a general tensorial property of $\phi$:

$$\nabla \cdot (\mathbf{u}\phi) - \nabla \cdot (\gamma \nabla \phi) = S_\phi(\phi) \tag{1}$$

where, for convenience, the source term is linearized in the following way:

$$S_\phi(\phi) = S - L\phi \tag{2}$$

In shortest terms, the FV discretization uses the integral form of the above equation,

$$\int_{V_P} \nabla \cdot (\mathbf{u}\phi)\, dV - \int_{V_P} \nabla \cdot (\gamma \nabla \phi)\, dV = \int_{V_P} S_\phi(\phi)\, dV \tag{3}$$

over the control volume (CV) around the point $P$, located in its center, Figure 1.

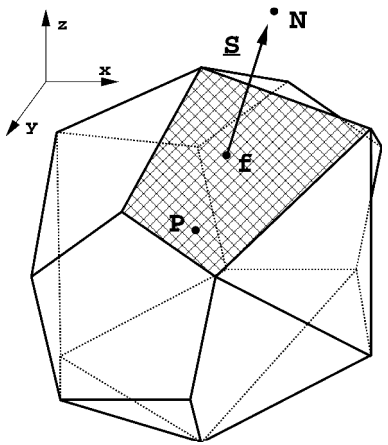


**Figure 1.** Control volume.

A second-order-accurate approximation of the integrals in Eq. (3) is obtained by assuming a linear variation of $\phi$ around $P$:

$$\phi(\mathbf{x}) = \phi_P + (\mathbf{x} - \mathbf{x}_P) \cdot (\nabla\phi)_P \tag{4}$$

where

$$\phi_P = \phi(\mathbf{x}_P) \qquad (\nabla\phi)_P = \nabla\phi(\mathbf{x}_P) \tag{5}$$

This is the major source of numerical errors. If a better solution is needed, CVs should be subdivided such that the assumption of linear variation becomes acceptable.

When Eq. (4) is used to evaluate the integrals in Eq. (3), the following form of the discretized transport equation is obtained:

$$\sum_f F\phi_f - \sum_f \gamma_f \mathbf{s} \cdot (\nabla\phi)_f = SV_P - LV_P\phi_P \tag{6}$$

where $f$ represents the cell face (and face interpolate) and $\mathbf{s}$ is the outward-pointing face area vector (with regard to $P$) between cells $P$ and $N$. The face values of $\phi$ and $\mathbf{s} \cdot \nabla\phi$ are calculated as follows:

$$\phi_f = f_x\phi_P + (1 - f_x)\phi_N \tag{7}$$

$$\mathbf{s} \cdot (\nabla\phi)_f = |\Delta| \frac{\phi_N - \phi_P}{|\mathbf{d}|} + \mathbf{k} \cdot (\nabla\phi)_f \tag{8}$$

where $P$ and $N$ are the points around the face $f$, $f_x$ is the interpolation factor, and $\Delta$ and $\mathbf{k}$ represent the nonorthogonal decomposition [25] of $\mathbf{s}$ such that

$$\mathbf{s} = \Delta + \mathbf{k} \tag{9}$$

$F$ in Eq. (6) is the face convection flux which satisfies the continuity constraint (if any):

$$F = \mathbf{s} \cdot \mathbf{u}_f \tag{10}$$

Downloaded by [McGill University Library] at 05:35 06 October 2012

The cell gradients of $\phi$ are calculated using the generalized Gauss' theorem in its second-order-accurate discretized form:

$$\int_V \nabla\phi \, dV = \oint_{\partial V} d\mathbf{s} \, \phi = \frac{1}{V_P} \sum_f \mathbf{s}\phi_f \tag{11}$$

Combining Eqs. (6), (7), (8), (10), and (11), an algebraic equation is obtained for each CV:

$$a_P\phi_P + \sum_N a_N\phi_N = R_P \tag{12}$$

thus creating a system of algebraic equations,

$$[A][\phi] = [R] \tag{13}$$

where $[A]$ is a sparse matrix, $[\phi]$ is the vector of $\phi$s for all CVs, and $[R]$ is the right-hand-side vector.

Downloaded by [McGill University Library] at 05:35 06 October 2012

## 3. TAYLOR SERIES TRUNCATION ERROR ANALYSIS

The first group of error estimates is based on the Taylor series analysis of the solution, where the discretization process is considered as a truncation of the infinite series. The truncated form of the Taylor expansion at the point $P$ is used to describe the solution over the CV surrounding it [see Eq. (4)] and the complete solution is created as a union of these locally defined "shape functions."

Consider the Taylor series expansion in space of a function around $P$:

$$\begin{aligned}\phi(\mathbf{x}) = \phi_P &+ (\mathbf{x}-\mathbf{x}_P)\cdot(\nabla\phi)_P + \frac{1}{2}(\mathbf{x}-\mathbf{x}_P)^2 : (\nabla\nabla\phi)_P \\ &+ \frac{1}{3!}(\mathbf{x}-\mathbf{x}_P)^3 :: (\nabla\nabla\nabla\phi)_P \\ &+ \cdots + \frac{1}{n!}(\mathbf{x}-\mathbf{x}_P)^n \underbrace{:::}_{n} (\underbrace{\nabla\nabla\cdots\nabla}_{n}\phi)_P + \cdots\end{aligned} \tag{14}$$

Here, $(\mathbf{x}-\mathbf{x}_P)^n$ represents the $n$th tensorial product of the vector $(\mathbf{x}-\mathbf{x}_P)$ with itself, producing an $n$th-rank tensor. The operator "$\underbrace{:::}_{n}$" is the $n$th inner product of two $n$th-rank tensors, creating a scalar.

A $p$th-order-accurate discretization method describes the local variation of $\phi$ with the first $p$ terms of the Taylor series. The discretization error can therefore also be expressed as an (infinite) series in higher derivatives of $\phi$:

$$e(\mathbf{x}) = \Phi(\mathbf{x}) - \phi(\mathbf{x}) = \sum_{n=p}^{\infty} \frac{1}{n!}(\mathbf{x}-\mathbf{x}_P)^n \underbrace{:::}_{n} (\underbrace{\nabla\nabla\cdots\nabla}_{n}\phi)_P \tag{15}$$

where $\Phi(\mathbf{x})$ is the exact solution. The error estimate is therefore

$$e_t(\phi) = \left| \frac{1}{V_P} \int_V \left[ \sum_{n=p}^{\infty} \frac{1}{n!} (\mathbf{x} - \mathbf{x}_P)^n \underbrace{:::}_{n} (\underbrace{\nabla\nabla\cdots\nabla}_{n} \phi)_P \right] dV \right|$$

$$\leq \frac{1}{V_P} \sum_{n=p}^{\infty} \left| \int_{V_P} \left( \frac{1}{n!} (\mathbf{x} - \mathbf{x}_P)^n \underbrace{:::}_{n} (\underbrace{\nabla\nabla\cdots\nabla}_{n} \phi)_P \right) dV \right| \tag{16}$$

If the exact solution $\Phi(\mathbf{x})$ is smooth and the CV is small, contributions from higher terms of the expansion in Eq. (16) decrease rapidly with increasing $n$. Thus, the error estimate uses only the first term of the expansion, which after some rearrangements reads:

$$e_t(\phi) = \frac{1}{V_P} \frac{1}{p!} \left| \left[ \int_{V_P} (\mathbf{x} - \mathbf{x}_P)^p \, dV \right] \underbrace{:::}_{p} (\underbrace{\nabla\nabla\cdots\nabla}_{p} \phi)_P \right| \tag{17}$$

If the mesh is too coarse (i.e., the solution is not smooth on the mesh scale), the contribution of higher-order terms can be significant and Eq. (17) underestimates the error.

For second-order-accurate FV discretization, the prescribed spatial variation of $\phi$ over the CV is linear, Eq. (4), and the error estimate is

$$e_t(\phi) = \frac{1}{V_P} \frac{1}{2} \left| \left[ \int_{V_P} (\mathbf{x} - \mathbf{x}_P)^2 \, dV \right] : (\nabla\nabla\phi)_P \right| = \frac{1}{2V_P} |\mathbf{M} : (\nabla\nabla\phi)_P| \tag{18}$$

where $\mathbf{M}$ in Eq. (18) is the second geometric moment tensor for the CV:

$$\mathbf{M} = \int_{V_P} (\mathbf{x} - \mathbf{x}_P)^2 \, dV \tag{19}$$

The error from Eq. (18) can be estimated in several ways. The first is the well-established Richardson extrapolation [15, 17, 21, 23, 24], which uses numerical solutions from two meshes with different spacings. The new error estimate, presented in Section 3.2, estimates the error from a single solution by evaluating Eq. (18) directly.

### 3.1. Richardson Extrapolation

The basic idea of Richardson extrapolation is to obtain an approximation of the leading term in Eq. (17) from suitably weighted solutions on two meshes with different spacings [26, 27].

The spatial variation of the exact solution on meshes with spacing $h_1$ and $h_2$ can be written symbolically as [26]

$$\Phi(\mathbf{x}) = \phi(\mathbf{x}, h_1) + h_1^p C(\mathbf{x}) + O(\mathbf{x}, h_1^q) \tag{20}$$

$$\Phi(\mathbf{x}) = \phi(\mathbf{x}, h_2) + h_2^p C(\mathbf{x}) + O(\mathbf{x}, h_2^q) \tag{21}$$

where $\phi(\mathbf{x}, h_i)$ is the approximate solution on the mesh with spacing $h_i$, $h_i^p C(\mathbf{x})$ is the leading term of the truncation error, $h$ is the local linear mesh size, $p$ is the order of discretization, and $O(\mathbf{x}, h_i^q)$ is the remainder of the truncation error. From Eqs. (20)

Downloaded by [McGill University Library] at 05:35 06 October 2012

and (21), $C(\mathbf{x})$ is approximated as

$$C(\mathbf{x}) = \frac{\phi(\mathbf{x}, h_2) - \phi(\mathbf{x}, h_1)}{h_1^p - h_2^p} \tag{22}$$

This can be used to improve the fine-mesh solution $\phi(\mathbf{x}, h_2)$ using Eq. (21). The improved ($q$th-order-accurate) solution is then used to estimate the error in $\phi(\mathbf{x}, h_2)$ (i.e., on the fine mesh!),

$$e_t(\phi) = |\phi(\mathbf{x}, h_2) + h_2^p C(\mathbf{x}) - \phi(\mathbf{x}, h_2)| = \frac{|\phi(\mathbf{x}, h_2) - \phi(\mathbf{x}, h_1)|}{(h_1/h_2)^p - 1} \tag{23}$$

or, for second-order-accurate discretization,

$$e_t(\phi) = \frac{|\phi(\mathbf{x}, h_2) - \phi(\mathbf{x}, h_1)|}{(h_1/h_2)^2 - 1} \tag{24}$$

It is instructive to analyze the relationship between Richardson extrapolation and Eq. (18) in the simplest case: a hexahedral CV aligned with the coordinate system, Figure 2, where $\mathbf{M}$ is simple to evaluate:

$$\mathbf{M} = \frac{V_P}{12}\begin{bmatrix} \Delta x^2 & 0 & 0 \\ 0 & \Delta y^2 & 0 \\ 0 & 0 & \Delta z^2 \end{bmatrix} \tag{25}$$

The error estimate, Eq. (18), simplifies to

$$e_t(\phi) = \frac{1}{24}\left|\Delta x^2\left(\frac{\partial^2\phi}{\partial x^2}\right)_P + \Delta y^2\left(\frac{\partial^2\phi}{\partial y^2}\right)_P + \Delta z^2\left(\frac{\partial^2\phi}{\partial z^2}\right)_P\right| \tag{26}$$

As $(\nabla\nabla\phi)_P$ is independent of the mesh, $|\mathbf{M}\colon(\nabla\nabla\phi)_P|$ scales quadratically with $h$. Richardson extrapolation uses this property to estimate the error, assuming that the magnitude of each term in $\mathbf{M}$ scales individually with $h^2$. This is valid only for geometrically similar CVs; if this is not the case, Richardson extrapolation loses accuracy.

Richardson extrapolation requires two solutions on meshes with different spacings, which is not always feasible in industrial applications. It also underestimates the solution error, particularly on coarse meshes; once the solution is smooth on both meshes, its accuracy improves rapidly.

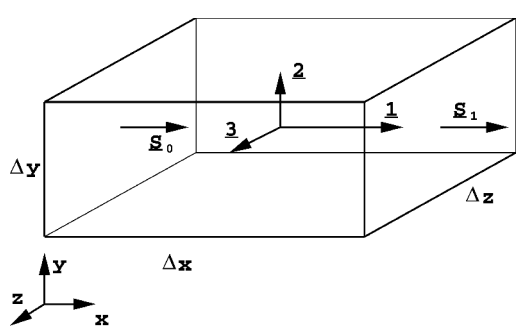


**Figure 2.** Hexahedral CV aligned with the coordinate system.

Downloaded by [McGill University Library] at 05:35 06 October 2012

### 3.2. Taylor Series Error Estimate

It is possible to obtain an estimate of the error from a single solution, a novel approach to Taylor series error estimation. The terms in Eq. (18) are approximated from the available solution and the mesh geometry.

The task of creating a single-mesh truncation error estimate can be divided into two parts: estimating the second gradient of $\phi$ in $P$ and evaluating $\mathbf{M}$ for a nontrivially shaped CV.

The $(\nabla\nabla\phi)_P$ is calculated using Gauss' theorem twice. This, in fact, only provides the average second gradient, whereas Eq. (18) requires the value in the centroid of the CV. As a consequence, the estimate will be accurate only if the solution is smooth relative to the mesh size.

The calculation of $\mathbf{M}$ for CVs in an arbitrarily unstructured mesh follows the work of Helf and Küster [28]. Using Gauss' theorem, the volume integral in Eq. (19) is reduced to a set of geometric moment integrals over the faces and finally to integrals over the edges.

$$\mathbf{M} = \int_{V_P} (\mathbf{xx})\, dV = \frac{1}{3} \int_{V_P} \nabla \cdot [\mathbf{x}(\mathbf{xx})]\, dV = \frac{1}{3} \sum_f \int_{S_f} (d\mathbf{s} \cdot \mathbf{x})(\mathbf{xx}) \tag{27}$$

If the faces are flat, $d\mathbf{s} \cdot \mathbf{x}$ reduces further:

$$\int_{S_f} (d\mathbf{s} \cdot \mathbf{x})(\mathbf{xx}) = \hat{\mathbf{S}} \cdot \mathbf{x}_f \int_{S_f} (\mathbf{xx})\, dA \tag{28}$$

Repeating the procedure once again, the second geometric moment for the face reduces to a sum of integrals over face edges, which are easily calculated.

Having in mind the limited accuracy of $(\nabla\nabla\phi)_P$, it would be wise to produce a simpler estimate of $\mathbf{M}$. If the orientation of the coordinate system were chosen to coincide with the principal geometric axes of inertia for the CV, $\mathbf{M}$ would reduce to diagonal-only and $\mathbf{M} : (\nabla\nabla\phi)_P$ would be similar to Eq. (26). For a hexahedral cell of arbitrary orientation, vectors **1**, **2**, and **3** can be approximated from the face area vectors of the opposite face pairs. Thus, for example, **1** is approximated with (Figure 2)

$$\mathbf{1} = \left( \frac{\mathbf{s}_0}{|\mathbf{s}_0|} + \frac{\mathbf{s}_1}{|\mathbf{s}_1|} \right) \frac{2V_P}{|\mathbf{s}_0| + |\mathbf{s}_1|} \tag{29}$$

and the error estimate, Eq. (18), simplifies to

$$e_l(\phi) = \frac{1}{24V_P} \left| \mathbf{1} \cdot (\mathbf{1} \cdot (\nabla\nabla\phi)_P) + \mathbf{2} \cdot (\mathbf{2} \cdot (\nabla\nabla\phi)_P) + \mathbf{3} \cdot (\mathbf{3} \cdot (\nabla\nabla\phi)_P) \right| \tag{30}$$

The off-diagonal terms in $\mathbf{M}$ are neglected, but at least the cell aspect ratio is taken into account. This principle can be extended to general polyhedral shapes by introducing an "orientation vector," defined as the ratio of cell volume and the average cell cross section in a given direction.

Downloaded by [McGill University Library] at 05:35 06 October 2012

One can, of course, go even further: assuming that the CV is not distorted at all, the error scales with $h^2$ and the magnitude of $(\nabla\nabla\phi)_P$,

$$e_t(\phi) = \frac{1}{24} h^2 \sqrt{(\nabla\nabla\phi)_P : (\nabla\nabla\phi)_P} \tag{31}$$

which further reduces the accuracy of the estimate because the information on the shape of the CV is lost. Having in mind the situations of mesh-to-flow alignment and high cell aspect ratios regularly used in CFD, Eq. (30) is chosen as a good balance of accuracy and computational cost.

Downloaded by [McGill University Library] at 05:35 06 October 2012

## 4. MOMENT ERROR ESTIMATE

The second novel error estimate will be derived from using an interesting property of the exact solution: if the original transport equation is satisfied in its differential form, all transport equations for higher moments of $\phi$ are also satisfied. A similar idea has been suggested in [16], but never fully developed. At this stage, we shall limit ourselves to the second moment of $\phi$:

$$m_\phi = \frac{1}{2}\phi^2 \tag{32}$$

The transport equation for $m_\phi$, derived from Eqs. (3) and (32), reads:

$$\nabla\cdot(\mathbf{u}m_\phi) - \nabla\cdot(\gamma\nabla m_\phi) = S_\phi(\phi)\phi - \gamma(\nabla\phi\cdot\nabla\phi) \tag{33}$$

As stated before, the FV discretization produces a solution which satisfies Eq. (3) over each CV in the integral form. This solution is, however, of limited accuracy: there is no quarantee that Eq. (33) will also be satisfied. The imbalance in the integral form of Eq. (33) depends on the local discretization error:

$$r_P = \int_{V_P} [\nabla\cdot(\mathbf{u}m_\phi) - \nabla\cdot(\gamma\nabla m_\phi) - S_\phi(\phi)\phi + \gamma(\nabla\phi\cdot\nabla\phi)]\, dV \tag{34}$$

Here, the cell values of $m_\phi$ are calculated from $\phi_P$ using Eq. (32). Convection, diffusion, and source terms are assembled following the discretization practice outlined in Section 2. On boundaries, $m_\phi$ is calculated consistently with the prescribed boundary conditions.

The same principle is used on vector (tensor) transport equations, where the second moment is defined as the inner product of the tensor with itself and the cell imbalance is constructed as before. Unlike the TSEE, the MEE always produces a scalar error. For vectors and tensors, the estimate corresponds to the error in the magnitude (norm) of the variable.

### 4.1. Normalization of the Moment Error Estimate

The dimensions of $r_P$ in Eq. (34) are $[\phi]^2[L]^3/[T]$, i.e., it does not correspond to the absolute error in $\phi$. In order to obtain the absolute error magnitude, a suitable normalization practice is required. The normalization is based on the local transport

conditions:

$$u_t = |\mathbf{u}| + \frac{\gamma}{h} \tag{35}$$

where $h$ is the local mesh size. The characteristic time scale $T$ is then

$$T = \frac{h}{u_t} = \frac{h^2}{|\mathbf{u}|h + \gamma} \tag{36}$$

Combining Eqs. (36) and (34) gives the final form of the MEE, with the same dimensions as $\phi$:

$$e_m(\phi) = 2\sqrt{\frac{|r_P|T}{V_P}} \tag{37}$$

The MEE is cheap to compute and its behavior on coarse meshes, as will be shown later, is significantly better than that of the TSEE. The main disadvantage of this method is its relative inaccuracy on very fine meshes. This is caused by the fact that the balance equation for $m_\phi$ uses not only the value but also the gradient of $\phi$, which, for zero estimated error, should also be exact.

Downloaded by [McGill University Library] at 05:35 06 October 2012

## 5. NUMERICAL EXAMPLES

In order to examine the accuracy of the two novel error estimates, two numerical examples with analytical solutions will be presented. Although the selected cases do not represent "real" flow situations, they provide useful insight into the accuracy and scaling properties of the new error estimates.

### 5.1. Point Source in Cross-Flow

Consider the case of convection-diffusion of a passive scalar from a fixed-strength point source in a uniform velocity field. The 2-D analytical solution can be found in [29]:

$$\phi(x, y) = \frac{S^*}{2\pi\gamma} K_0\left(\frac{U_1\sqrt{x^2 + y^2}}{2\gamma}\right) e^{(U_1 x/2\gamma)}$$

Here, $x$ and $y$ are the spatial coordinates with the origin at the source, and the $x$ pointing in the direction of the convection velocity; $S^* = 16.67[\phi]/\text{s}$ is the strength of the source, $\gamma = 0.05\ \text{m}^2/\text{s}$ is the effective diffusion, $U_1 = 1\ \text{m/s}$ is the $x$ component of the velocity and $K_0$ is the modified Bessel function of the second kind and zero order. In order to avoid the singularity, the point source is located outside the computational domain. The problem will be solved on a series of uniformly refined meshes. Two situations of mesh-to-flow alignment will be presented: a uniform orthogonal mesh aligned with the flow; and a nonuniform, nonaligned, nonorthogonal mesh.

Downloaded by [McGill University Library] at 05:35 06 October 2012

**5.1.1. Mesh aligned with the flow.** The test setup, Figure 3, consists of a $4\times1$ m domain located 0.05 m downstream of the source. The analytical solution is prescribed on fixed value boundaries. Meshes used in this comparison range from 50 to 51,520 CVs.

Figure 4*a* shows the exact solution on the $80\times41$ CVs. The distribution of the exact and estimated errors is given in Figure 4. Two parts of the exact error can be recognized. The region of the highest exact error corresponds to the highest estimated error and is accurately detected by both error estimates. Downstream, the exact error is still large, but the estimates do not pick up its source, as the error is transported from upstream: this nonlocal error cannot be detected by the estimate. As the mechanism of error transport is not fully understood, we shall assume that the error source creates only a local error. The results in the present study show that this simplification does not seriously degrade the accuracy of error estimation.

Figure 5 shows the reduction of the mean and maximum error with the number of CVs. It is expected that the error reduces with the square of the mesh size, following the second-order accuracy of the method. In two spatial dimensions, the number of computational points quadruples if the mesh spacing is halved in each direction. The slope of the curve in Figure 5*a* should therefore be $-1$. Figure 5 also illustrates the usefulness of the proposed pair of error estimates. On coarse meshes, the MEE shows superior accuracy, whereas the TSEE underpredicts the error level. The average of the two estimates shows remarkable accuracy on all meshes.

**5.1.2. Nonorthogonal, nonaligned mesh.** Let us now consider the effects of mesh-to-flow alignment and nonorthogonality on the accuracy of the solution. In the first instance, second-order central differencing (CD) will be used for the convection term. The test setup for this situation is given in Figure 6. The dimensions of the domain are $3\times1.41$ m, with the same diffusion coefficient and relative position to the source as above.

The exact solution on the $40\times40$ CVs mesh together with the exact and estimated error distribution are given in Figure 7. Both error estimates pick up the error source well. The scaling of the exact and estimated error with the mesh size is shown in Figures 8*a* and 8*b*.

In the case of mean error, both estimates show comparable accuracy. The TSEE slightly underestimates the error, whereas the MEE again loses accuracy

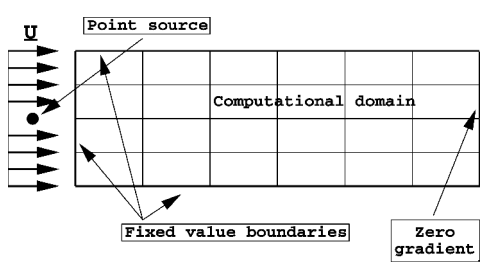


**Figure 3.** Point source in cross-flow: mesh aligned with the flow.

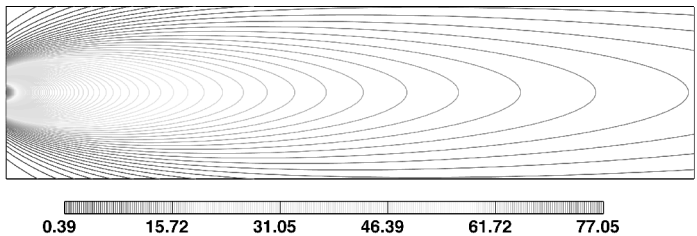


(a) Exact solution.

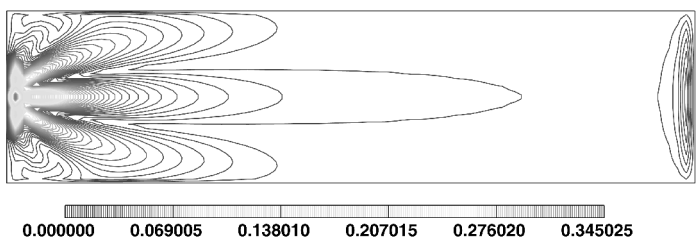


(b) Exact error magnitude.

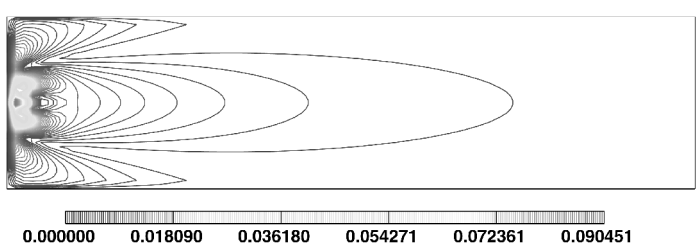


(c) Taylor Series Error estimate.

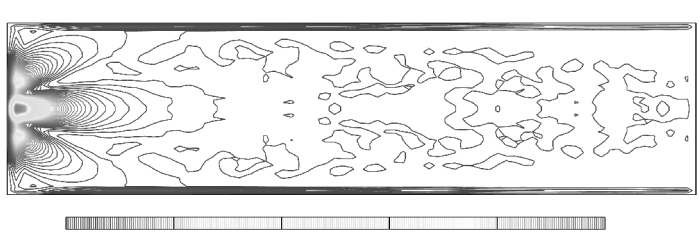


(d) Moment Error estimate.

**Figure 4.** Aligned mesh: exact and estimated errors. (*a*) Exact solution. (*b*) Exact error magnitude. (*c*) Taylor series error estimate. (*d*) Moment error estimate.

Downloaded by [McGill University Library] at 05:35 06 October 2012

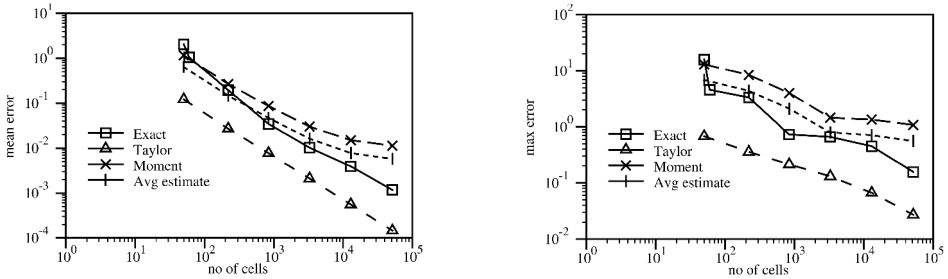


(a) Mean error. (b) Maximum error.

**Figure 5.** Aligned mesh: scaling of the error. (*a*) Mean error. (*b*) Maximum error.

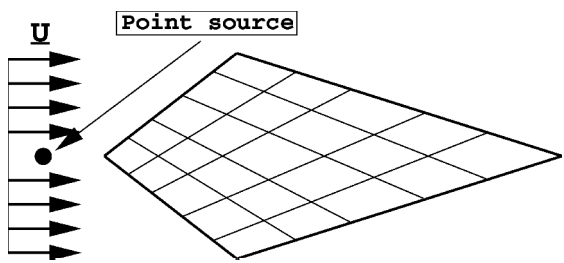


**Figure 6.** Point source in cross-flow: nonorthogonal, nonaligned mesh.

on very fine meshes. Discretization errors introduced by mesh distortion do not noticeably change the rate of error reduction with mesh refinement.

In order to introduce more numerical diffusion, upwind differencing (UD) is used for the convection term. The scaling of the mean and maximum error is shown in Figures 8*c* and 8*d*. The slope of the curve is now closer to $-\frac{1}{2}$, compared with $-1$ for CD. Both the mean and maximum error are now much higher, illustrating the importance of second-order convection discretization.

Error estimates, however, do not follow the scaling behavior of the error. Numerical diffusion smears the gradients, thus producing the picture of a smoothly varying field. In effect, the quality of the solution is so bad that accurate error estimation is not possible. It should be noted that the MEE shows slightly slower error reduction with refinement. This is, however, a very severe test for error estimates, with a combination of poor mesh quality, high discretization errors, and steep gradients in the solution.

## 5.2. Point Jet

In order to test the behavior of error estimates on a fluid flow situation, a point jet in 2-D is considered. The analytical solution [30] for the coordinate system located

Downloaded by [McGill University Library] at 05:35 06 October 2012

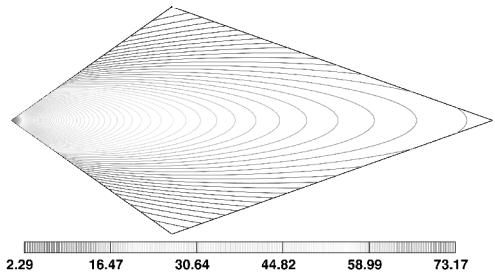


(a) Exact solution.

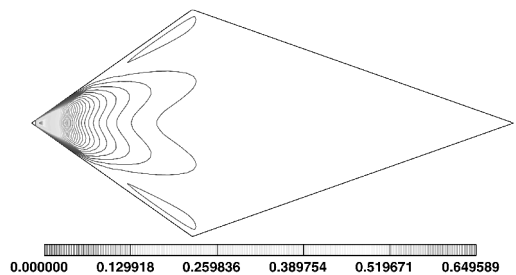


(b) Exact error magnitude.

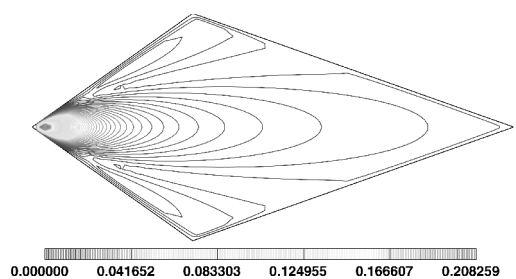


(c) Taylor Series Error estimate.

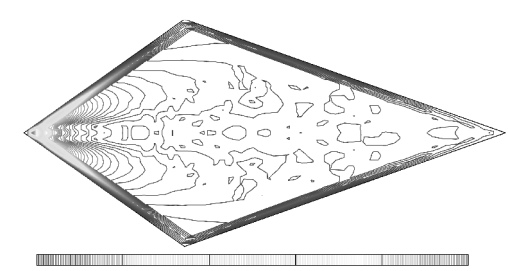


(d) Moment Error estimate.

**Figure 7.** Nonaligned mesh: exact estimated errors. (*a*) Exact solution. (*b*) Exact error magnitude. (*c*) Taylor series error estimate. (d) Moment error estimate.

Downloaded by [McGill University Library] at 05:35 06 October 2012

Downloaded by [McGill University Library] at 05:35 06 October 2012

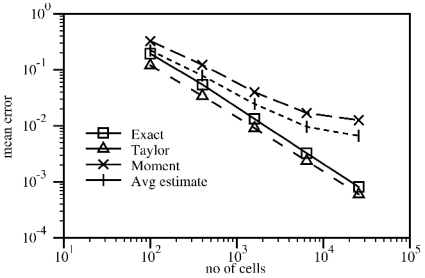


(a) Main error with CD.

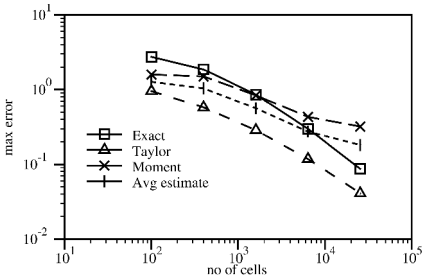


(b) Maximum error with CD.

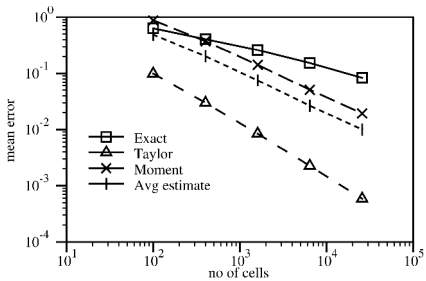


(c) Mean error with UD.

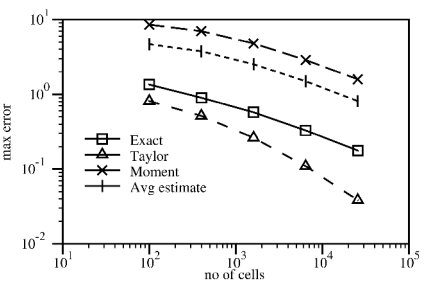


(d) Maximum error with UD.

**Figure 8.** Nonaligned mesh: scaling of the error. (*a*) Mean error with CD. (*b*) Maximum error with CD. (*c*) Mean error with UD. (*d*) Maximum error with UD.

at the mouth of the orifice with **i** pointing downstream is

$$\mathbf{u} = u\mathbf{i} + v\mathbf{j} \tag{39}$$

$$u = \frac{A}{B}x^{-1/3}\,\operatorname{sech}^2\left(x^{-2/3}\frac{y}{B}\right) \tag{40}$$

$$v = -\frac{1}{3}Ax^{-2/3}\tanh^2\left(x^{-2/3}\frac{y}{B}\right) + \frac{2}{3}x^{-4/3}y\,\operatorname{sech}^2\left(x^{-2/3}\frac{y}{B}\right) \tag{41}$$

$$A = \left(\frac{9}{2}\nu M_j\right)^{1/3} \qquad B = \left(\frac{48\nu^2}{M_j}\right)^{1/3} \tag{42}$$

where $M_j = U_0^2 D$ is the momentum carried by the jet.

The domain is 4×1 m in size, 0.5 m downstream of the orifice, aligned with **i**, and utilizes the symmetry of the problem. In order to simplify the discussion, only the magnitude of the estimated and exact error are presented.

The exact solution and the exact and estimated errors on the 80×41 CVs are given in Figure 9. Highest error is associated with the high gradients in the vicinity of the source. In the rest of the domain, errors are relatively low. The new error

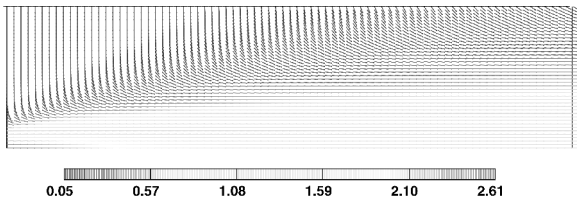


(a) Exact solution.

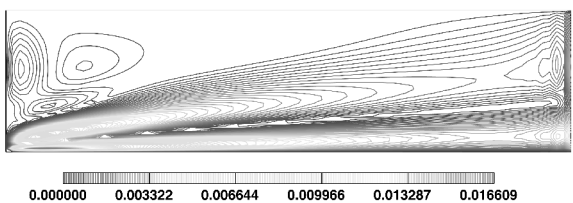


(b) Exact error magnitude.

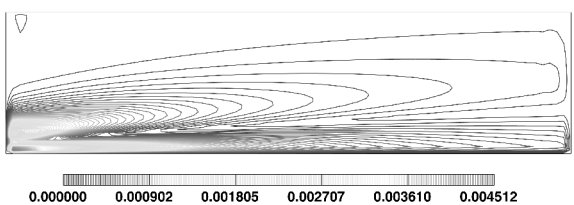


(c) Taylor Series Error estimate.

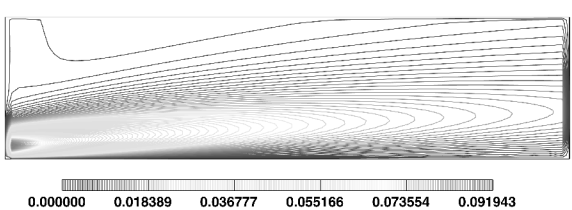


(d) Moment Error estimate.

**Figure 9.** Point jet: exact and estimated errors. (*a*) Exact solution. (*b*) Exact error magnitude. (*c*) Taylor series error estimate. (*d*) Moment error estimate.

Downloaded by [McGill University Library] at 05:35 06 October 2012

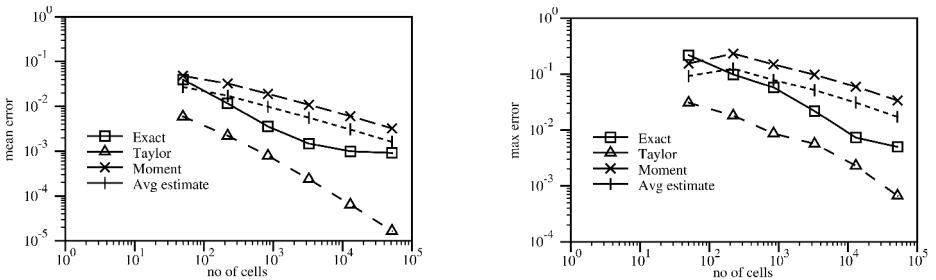


(a) Mean error. (b) Maximum error.

**Figure 10.** Point jet: scaling of the error. (*a*) Mean error. (*b*) Maximum error.

Downloaded by [McGill University Library] at 05:35 06 October 2012

estimates pinpoint the regions of high error well. A slight anomaly in the error distribution for the MEE in Figure 9*d* has been traced to the lower order of accuracy associated with fixed-value boundaries, where the face compensation of fourth-order terms of the MEE is lost. The terms in question are large on the inlet side of the domain because of high gradients in **u**.

The scaling of the mean and maximum error shown in Figure 10 exhibits several interesting features. On very fine meshes, the exact solution does not follow the expected error scaling. Here, the error is extremely low in large regions and further refinement has no effect. At the same time, the error is still large in the vicinity of the jet and controls the scaling of the mean error. Although it shows remarkable accuracy on coarse meshes, the MEE overestimates both the mean and maximum errors. Its error reduction rate is lower than for the TSEE because of the accuracy problems at the inlet boundary. The TSEE, on the other hand, consistently underestimates the error. In spite of that, the pair of estimates does a remarkably good job, both in bounding the exact error and in terms of absolute accuracy of the average estimated error.

## 6. SUMMARY

Automatic resolution control relies on an a-posteriori error estimate for the information about the distribution of the discretization error. Its effectiveness therefore depends on the quality of the selected estimate. This article deals with the issue of error estimation, thus setting a foundation for the overall adaptive procedure which will be described and tested in the following articles [31, 32].

Initially, properties of a good error estimate have been outlined, together with the difference between error indicators and error estimates. The main objective of the work presented here was to create an error estimate with the same dimensionality as the solution variable, making it practical and easy to use. Two novel error estimates have been proposed: the Taylor series error estimate (TSEE), based on the truncation error analysis; and the moment error estimate (MEE), based on the higher moment imbalance.

Unlike the more popular Richardson extrapolation, the TSEE uses only a single solution in order to estimate the error. Although the TSEE seems to be a straightforward way of estimating the discretization error, it suffers from several deficiencies. It uses an estimate of the second gradient of the transported variable and its scalar product with the geometric moment tensor for the CV. Although the error can be calculated on a cell-by-cell basis, the error estimate is still considered relatively expensive, as it requires a product of two second-rank tensors. A simple and cheaper approximate procedure of comparable accuracy is proposed and tested on two model problems. The TSEE typically underestimates the error, as a consequence of the fact that the double Gauss' theorem used to calculate the second gradient produces the average value of the gradient over the nearest neighbors, rather than the required cell-center value.

The MEE does not follow the traditional truncation error analysis: instead, it relies on the fact that the exact solution of the transport equation for a general variable $\phi$ also satisfies the transport equations for all higher moments of $\phi$. It is therefore possible to examine the numerical imbalance in higher moments over every CV in order to estimate the discretization error. The imbalance is then normalized in an appropriate way in order to obtain the absolute error magnitude in $\phi$.

Unlike the TSEE, the MEE consistently overestimates the error. Its accuracy is better, but its real potential can be seen when two estimates are used together. As the presented test cases show, two error estimates bound the error and their average estimates its absolute magnitude with reasonable accuracy.

Accurate error estimation is a basis for an effective adaptive refinement procedure, which will be described and tested in the following article [31].

Downloaded by [McGill University Library] at 05:35 06 October 2012

## REFERENCES

1. Ž. Lilek and M. Perić, A Fourth-Order Finite Volume Method with Colocated Variable Arrangement, *Comput. Fluids*, vol. 24, no. 3, pp. 239–252, 1995.
2. M. J. Berger and J. Oliger, Adaptive Mesh Refinement for Hyperbolic Partial Differential Equations, *J. Comput. Phys.*, vol. 53, pp. 484–512, 1984.
3. M. J. Berger and P. Collela, Local Adaptive Mesh Refinement for Shock Hydrodynamics, *J. Comput. Phys.*, vol. 82, pp. 64–84, 1989.
4. M. J. Berger and A. Jameson, Adaptive Multigrid Method for the Euler Equations, *Lect. Notes Phys.*, vol. 218, pp. 92–97, 1985.
5. H. A. Dwyer, Grid Adaptation for Problems in Fluid Dynamics, *AIAA J.*, vol. 22, no. 12, pp. 1705–1712, 1984.
6. W. Speares and E. F. Toro, A High Resolution Algorithm for Time Dependent Shock Dominated Problems with Adaptive Mesh Refinement, *Z. Flugwiss. Weltraumforsch.*, vol. 19, pp. 267–281, 1995.
7. R. Löhner, An Adaptive Finite Element Scheme for Transient Problems in CFD, *Comput. Meth. Appl. Mech. Eng.*, vol. 61, pp. 323–338, 1987.
8. R. Ramakrishnan, K. S. Bey, and E. A. Thornton, Adaptive Quadrilateral and Triangular Finite Element Scheme for Compressible Flows, *AIAA J.*, vol. 28, pp. 51–59, 1990.
9. M. J. Berger and A. Jameson, Automatic Adaptive Grid Refinement for the Euler Equations, *AIAA J.*, vol. 23, no. 4, pp. 561–568, 1985.
10. D. C. Catharell, A Solution-Adaptive-Grid Procedure for Transonic Flow Around Airfoils, *Tech. Rep. 88020*, Royal Aerospace Establishment, 1988.

11. W. Speares and E. F. Toro, A High-Resolution Algorithm for Time-Dependent Shock Dominated Problems with Adaptive Mesh Refinement, *Z. Flugwiss. Weltraumforsch.*, vol. 19, no. 4, pp. 267–281, 1995.
12. T. Sonar, V. Hannemann, and D. Hempel, Dynamic Adaptivity and Residual Control in Unsteady Compressible Flow Computation, *Math. Comput. Model.*, vol. 20, no. 10–11, pp. 201–213, 1994.
13. J. J. McGuirk, A. M. P. K. Taylor, and J. H. Whitelaw, The Assessment of Numerical Diffusion in the Upwind-Difference Calculations of Turbulent Recirculating Flows, in L. J. S. Bradbury, F. Durst, B. E. Launder, F. W. Schmidt, and J. H. Whitelaw (eds.), *Selected Papers from the Third International Symposium on Turbulent Shear Flows*, volume 3 of *Turbulent Shear Flows*, pp. 206–224, University of California, Davis, Sept. 9–11, 1981.
14. P. Tattersall and J. J. McGuirk, Evaluation of Numerical Diffusion Effects in Viscous Flow Calculation, *Comput. Fluids*, vol. 23, no. 1, pp. 177–209, 1994.
15. W. L. Chen, F. S. Lien, and M. Z. Leschziner, A Local Grid Refinement Scheme within a Multiblock Structured-Grid Strategy for General Flows, in *6th Int. Symp. on CFD*, Lake Tahoe, CA, September 1995.
16. D. C. Haworth, S. H. El Tahry, and M. S. Huebler, A Global Approach to Error Estimation and Physical Diagnostics in Multidimensional Fluid Dynamics, *Int. J. Numer. Meth. Fluids*, vol. 17, no. 1, pp. 75–97, 1993.
17. S. Muzaferija and D. Gosman, Finite-Volume CFD Procedure and Adaptive Error Control Strategy for Grids of Arbitrary Topology, *J. Comput. Phys.*, vol. 138, no. 2, pp. 766–787, 1997.
18. D. Ait-Ali-Yahia, W. G. Habashi, A. Tam, M.-G. Vallet, and M. Fortin, A Directionally Adaptive Methodology Using an Edge-Based Error Estimate on Quadrilateral Grids, *Int. J. Numer. Meth. Fluids*, vol. 23, pp. 673–690, 1996.
19. J. Dompierre, M.-G. Vallet, M. Fortin, Y. Bourgault, and W. G. Habashi, Anisotropic Mesh Adaptation: Towards a Solver and User Independent CFD, AIAA Paper 97-0861, 1997.
20. W. G. Habashi, J. Dompierre, and Y. Bourgault, Certifiable Computational Fluid Dynamics through Mesh Optimisation, *AIAA J.*, vol. 36, no. 5, pp. 703–711, 1998.
21. S. Caruso, J. H. Ferziger, and J. Oliger, Adaptive Grid Techniques for Elliptic Flow Problems, Tech. Rep. TF-23, Thermosci. Div. Stanford Univ. Stanford, CA, 1985.
22. F. Moukalled and S. Acharya, A Local Adaptive Grid Procedure for Incompressible Flows with Multigridding and Equidistribution Concepts, *Int. J. Numer. Meth. Fluids*, vol. 13, no. 9, pp. 1085–1111, 1991.
23. M. C. Thompson and J. H. Ferziger, An Adaptive Multigrid Technique for the Incompressible Navier-Stokes Equations, *J. Comput. Phys.*, vol. 82, pp. 94–121, 1989.
24. J. H. Ferziger and M. Perić, Further Discussion of Numerical Error in CFD, *Int. J. Numer. Meth. Fluids*, vol. 23, pp. 1–12, 1996.
25. H. Jasak, Error Analysis and Estimation in the Finite Volume Method with Applications to Fluid Flows, Ph.D. thesis, Imperial College, University of London, London, 1996.
26. S. Muzaferija, Adaptive Finite Volume Method for Flow Prediction Using Unstructured Meshes and Multigrid Approach, Ph.D. thesis, Imperial College, University of London, London, 1994.
27. J. H. Ferziger and M. Perić, *Computational Methods for Fluid Dynamics*, Springer-Verlag, Berlin–New York, 1995.
28. C. Helf and U. Küster, A Finite Volume Method with Arbitrary Polygonal Control Volumes and High Order Reconstruction for the Euler Equations, in S. Wagner, E. H. Hirschel, J. Périaux, and R. Piva (eds.), *Computational Fluid Dynamics*, pp. 234–238, Wiley, New York, 1994.

Downloaded by [McGill University Library] at 05:35 06 October 2012

29. J. O. Hinze, *Turbulence*, McGraw-Hill, New York, 1975.
30. R. L. Panton, *Incompressible Flow*, Wiley, New York, 1984.
31. H. Jasak and A. D. Gosman, Automatic Resolution Control for the Finite-Volume Method, Part 2: Adaptive Mesh Refinement, *Numer. Heat Transfer B*, vol. 38, no. 3, pp. 257–271, 2000.
32. H. Jasak and A. D. Gosman, Automatic Resolution Control for the Finite-Volume Method, Part 3: Turbulent Flow Applications, *Numer. Heat Transfer B*, vol. 38, no. 3, pp. 273–290, 2000.

Downloaded by [McGill University Library] at 05:35 06 October 2012